University of Nevada, Reno

Correlation between Acoustic Emission and Mechanoluminescence of Rock Cores under Quasistatic Compression

A thesis submitted in partial fulfillment
of the requirements for the degree of

Bachelor of Science in Physics and the Honors Program

by

Rachel A. Miller

Dr. Timothy Darling, Thesis Advisor

May, 2012

UNIVERSITY OF NEVADA RENO

THE HONORS PROGRAM

We recommend that the thesis
prepared under our supervision by

RACHEL A. MILLER

entitled

Correlation between Acoustic Emission and Mechanoluminescence of Rock Cores under Quasistatic Compression

be accepted in partial fulfillment of the
requirements for the degree of

BACHELOR OF SCIENCE

Timothy Darling, Ph.D., Advisor

W. Patrick Arnott, Ph.D., Committee Member

Tamara Valentine, Ph.D., Director, Honors Program

May, 2012

Abstract

When a rigid solid undergoes mechanical deformation, locally accumulated strain energy can be released through multiple avenues including acoustic emission (AE) and light emission known as mechanoluminescence (ML). In AE, events within a stressed rock such as defect movement, grain boundary shifting, and crack propagation create pressure waves which can be detected at the rock surface. While AE is used extensively for rock evaluation in geophysics, civil engineering, and mining, ML by comparison has received little attention from the geoscience community. ML from stressed and fracturing rock has been observed in mines, earthquakes, and the laboratory, but the underlying mechanism behind ML is poorly understood. Possible candidates include defect movement, creation of charged surfaces during fracturing of piezoelectric grains, and triboluminescence. Observing whether a correlation exists between ML and AE will help determine the source of ML. An apparatus for AE and ML detection of rock cores under quasistatic compression was designed and constructed. Using photomultiplier tubes and piezoelectric transducers, AE and ML events were spatially and temporally observed and correlated. AE and ML in Berea sandstone were measured, and, unexpectedly, the ML events were found to occur approximately 40 μs after the AE events.

Acknowledgements

I would first and foremost like to thank my advisor Dr. Timothy Darling for his guidance, encouragement, enthusiasm, and endless help. I would also like to gratefully acknowledge our machinist Wade Cline, whose time and skill contributed greatly to creating many of the parts used in this project. Appreciation is given to my committee members Dr. Pat Arnott, who first introduced me to experimental research, and Dr. Tamara Valentine for their time and advice. I would like to thank my parents for their continued support and encouragement and Muir for his helpful suggestions and endless patience. I would also like to thank Laura, who has warmly welcomed me into her family.

This research was made possible by funding from the UNR College of Science Research / Instructional Enhancement Award and by funding from the UNR Honors Undergraduate Research Award. The American Physical Society's Future of Physics Days March Travel Award contributed to the presentation of this research at the 2012 APS March Meeting. Appreciation is given to APS for the Outstanding Student Presentation Award received at the 2012 APS March Meeting.

Contents

List of Tables

List of Figures

Chapter 1

Acoustic Emission (AE)

1.1 Acoustic Emission Background

Many materials emit bursts of high frequency sound waves when under stress or deformation. These sound waves, known as acoustic emission (AE) or microseismic activity [7], are often a precursor to mechanical failure. For instance, a branch will emit sharp cracking noises shortly before breaking. When a rigid solid is stressed, local regions often exceed yield stresses long before the entire mass becomes unstable and fractures [10]. The locally accumulated strain energy can be released as AE.

By placing acoustic detectors on the stressed material, one can passively monitor local faults in materials undergoing deformation. AE has been used for several decades to study the structural integrity of geologic materials in civil engineering, geophysics, and mining. Sources of AE include defect movement, grain boundary shifting, and crack propagation [10].

1.2 Source Location Theory

The source of an acoustic emission event can be spatially and temporally located by using an array of multiple acoustic detectors. A given AE event creates a compressional wave (P-wave) which is detected by each detector at a recorded first arrival

time. The location and time of origination of the AE event can be determined if the following assumptions are made [11]:

1. The AE event originates as a point source.
2. The acoustic wave takes a straight path from the source to the detector.
3. The acoustic velocity is uniform and isotropic throughout the material.
4. Each set of first arrival times can be related to a single AE event.

The source location coordinates x_s, y_s, and z_s within the sample and the source time t_s can then be found by

$$(x_i - x_s)^2 + (y_i - y_s)^2 + (z_i - z_s)^2 = v^2(t_i - t_s)^2 \tag{1.1}$$

where t_i is the first arrival time and x_i, y_i, and z_i are the coordinates for a given acoustic detector ($i = 1, 2, 3, ..., n$ for n acoustic detectors) [7]. For a three-dimensional material, four detectors are required to obtain a unique solution for x_s, y_s, z_s, and t_s.

It is convenient to approximate a cylindrical rock core as a one-dimensional object, in which case y_s, z_s, y_i, and z_i can be neglected. Eq. (1.1) can then be written [7]

$$\pm(x_i - x_s) = v(t_i - t_s), \tag{1.2}$$

and only two detectors are required to obtain a unique solution for x_s and t_s. If it is assumed that $x_1 < x_2$ and the source lies at some point between two detectors mounted on the sample (Fig. 1.1), then

$$x_s - x_1 = v(t_1 - t_s), \tag{1.3}$$

$$x_2 - x_s = v(t_2 - t_s). \tag{1.4}$$

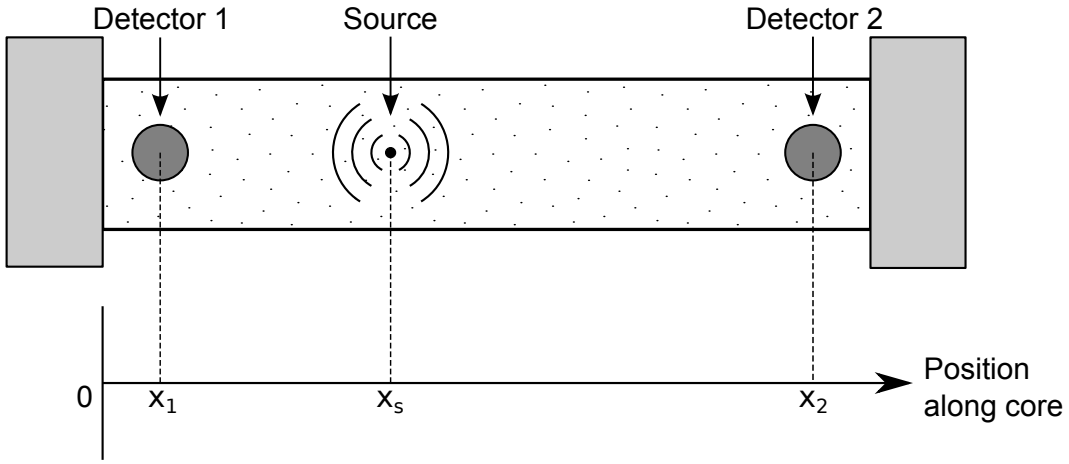

Figure 1.1: Linear source detection geometry for acoustic detectors placed directly on the sample. Adapted from [7].

With substitution, it can be shown that

$$x_s = \frac{v\Delta t + x_1 + x_2}{2} \tag{1.5}$$

where $\Delta t = t_1 - t_2$ [7]. This equation conveniently relates the difference in acoustic detection times to the source location. To obtain the source time, a little algebra yields

$$t_s = \frac{t_1 + t_2}{2} + \frac{x_1 - x_2}{2v}. \tag{1.6}$$

Eqs. (1.3) through (1.6) are only valid if the source originates between the two detectors. If the source is located outside the detectors,

$$\Delta t = \pm\frac{x_2 - x_1}{v} \tag{1.7}$$

and Δt does not depend on x_s. Therefore, the one-dimensional source detection method outlined above fails for acoustic emission events located outside the detec-

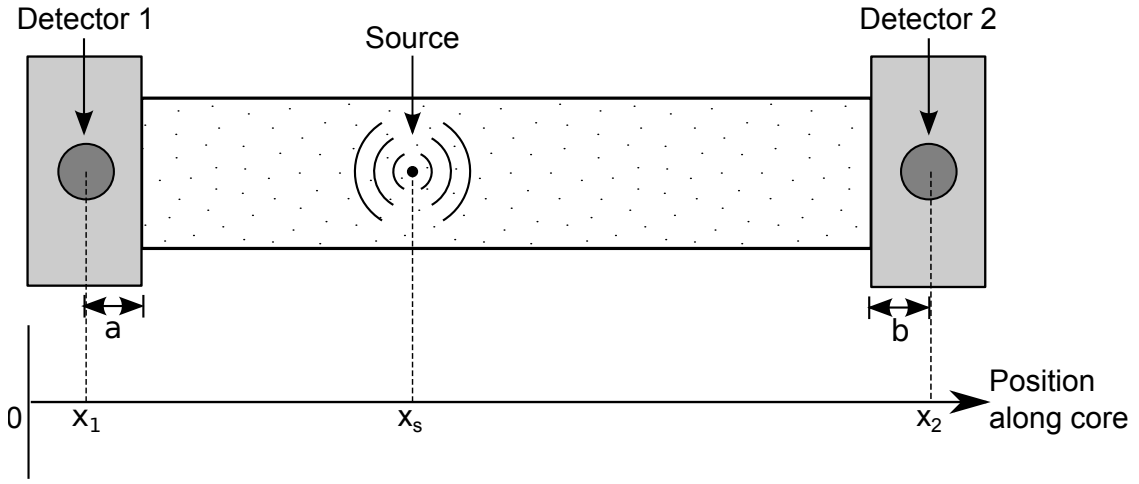

Figure 1.2: Linear source detection geometry for acoustic detectors placed on platens. Adapted from [7].

tors [7]. This is problematic, because a large amount of acoustic emission activity occurs at the rock core and platen boundary [7].

A relatively simple solution involves moving the detectors from the rock sample to the metal platens (Fig. 1.2). An additional advantage of this configuration is the detectors can be used repeatedly to measure multiple rock cores. Because the acoustic wave is now traveling through two different materials, the difference in sound velocity must be accounted for. Eq. (1.5) becomes

$$x_s = \frac{1}{2}\left[v\Delta t + x_1 + x_2 + (a-b)\left(\frac{c-v}{c}\right)\right] \tag{1.8}$$

where v is the sound velocity of the rock core, c is the sound velocity of the platens, a is the distance from the first detector to the rock core, and b is the distance from the second detector to the rock core [7]. Eq. (1.6) becomes

$$t_s = \frac{1}{2}\left[t_1 + t_2 + \frac{(x_1 - x_2)}{v} + \frac{(a+b)}{v} - \frac{(a+b)}{c}\right]. \tag{1.9}$$

Chapter 2

Mechanoluminescence (ML)

2.1 Mechanoluminescence Sources

Mechanoluminescence is the emission of light from a solid due to mechanical deformation, fracturing, rubbing, cutting, and crushing [16]. The terms used to describe mechanoluminescence are varied and often disputed. Several common terms are triboluminescence, which refers to light emission due to frictional rubbing, and piezoluminescence, which refers to light emission resulting from compression [12]. Fractoemission refers to the emission of photons and particles from a fractured surface [5]. In this work, mechanoluminescence, or ML, will be the preferred generic term as it describes light emission from a variety of mechanical sources.

Light is primarily created by two fundamental mechanisms: accelerating charges and atomic transitions. However, there are many ways to accelerate charges or to cause atomic transitions. Three likely sources of mechanoluminescence will be considered. The first source is the creation of fractures in a piezoelectric material. A piezoelectric material has a crystal structure without inversion symmetry. When a piezoelectric crystal is compressed, a charge difference is created across the crystal. If a piezoelectric material is fractured, the charge difference created across the crack can be great enough to cause a dielectric breakdown of the surrounding gas [5]. B.

P. Chandra estimates an electric field on the order of 10^7 to 10^8 V/m may be created between two oppositely charged new fracture surfaces [16]. This electric field would be enough to create a spark, as the dielectric strength of air is 3×10^6 V/m [15].

The second source of ML is from triboluminescence, or the creation of charged surfaces due to frictional rubbing. Light was observed by Wedgwood in 1792 by rubbing various quartz crystals and agates together [17, p. 37]. This triboluminescence is similar to the sparks created by rubbing socks across a carpet on a dry day. When two surfaces are rubbed together, localized charges can accumulate on these surfaces. These charges may create an electrical field great enough to cause a dielectric breakdown of the gas.

The third source of ML is defect movement within a grain. No natural crystal lattice is flawless. Every crystal has imperfections in its crystal lattice known as defects. Light emission due to defect movement has been studied extensively in alkali halide crystals (e.g. NaCl, KCl, KBr) [16, 3]. Defects in crystals can be created by exposure to X- and γ-radiation [8]. While pure alkali halide crystals are transparent, these defects absorb visible light and give the crystal a strong color [1]. Therefore, such defects are commonly referred to as color centers. For instance, table salt (NaCl) becomes a deep blue when exposed to γ-radiation. Similarly, quartz can gain a "smoky" color when exposed to γ-radiation [9]. ML from defect movement in colored alkali-halide crystals is likely a result of electron-hole recombination [16]. While X- and γ-radiation increase the number of defects in a crystal, small numbers of these defects occur naturally and may contribute to ML.

Both quartz and sugar are well known sources of mechanoluminescence [16]. Sugar exhibits a pale blue ML which can be seen by the unaided eye in a dark room. Sugar's ML spectrum has been shown to contain nitrogen discharge lines when surrounded by air, and neon spectral lines are seen when sugar is in a neon atmosphere [14].

Additionally, sugar is a piezoelectric material. Therefore, it is thought that the primary source of ML from sugar is the result of an electric discharge across air due to fracturing [6].

ML spectra from fractured quartz has been shown to contain nitrogen discharge lines [4], so rock ML may be due in part to gas discharge across piezoelectrically charged grains. Because rubbing quartz crystals together is known to create light [17], observed rock ML may be caused by frictional rubbing. While samples in this study have not been irradiated, small amounts of naturally occurring dislocations are likely still present within the crystal grains [12]. Therefore, defect movement is also a potential source of ML.

Whether acoustic emission is observed in conjunction with ML provides a clue to the source of the ML. Because fracturing of a material releases accumulated local stress energy, ML created during fracture is likely to result in an AE pulse originating at nearly the same time. ML originating from frictional rubbing of grains and fracture surfaces may occur on a variety of time scales and may be associated with fracture or with slow slip occuring during deformation. Therefore, ML from frictional rubbing may be associated with sharp AE pulses or with gradual acoustic background noise (i.e. "rumbling"). Defect movement may occur during deformation or fracture, so ML resulting from defect movement may occur in conjunction with AE or independently of AE.

Chapter 3

Apparatus Design

3.1 Light-Tight Chamber

The apparatus body is a cylindrical light-tight vacuum chamber (see Fig. 3.1). Sample cores were placed horizontally inside the chamber between two stainless-steel platens which applied uniaxial compressional stress to the sample. The amount of compression applied was controlled by a tightening a finely threaded screw. The frame which held the sample could be moved out of the chamber for sample loading (see Fig. 3.2). The apparatus could accommodate up to 6 photomultiplier tubes. Rock cores measuring up to 29 cm long and 3.8 cm in diameter could be tested. While rock samples were measured at atmospheric pressure, the vacuum-tight chamber will allow future experiments to be conducted in vacuum or in other gases.

The outer chamber was constructed from a stainless steel cylindrical tube measuring 2 ft. long and 4 in. in diameter. The chamber was sealed at each end by two ISO100 flanges. The inner frame supporting the sample was made from three threaded stainless steel rods that were welded to one flange. The opposite end of the frame was supported by a circular metal plate. Three teflon ovals were fastened to the end plate to guide the frame into position in the chamber (see Fig. 3.3). This design allowed for easy sliding of the frame out of and into the chamber.

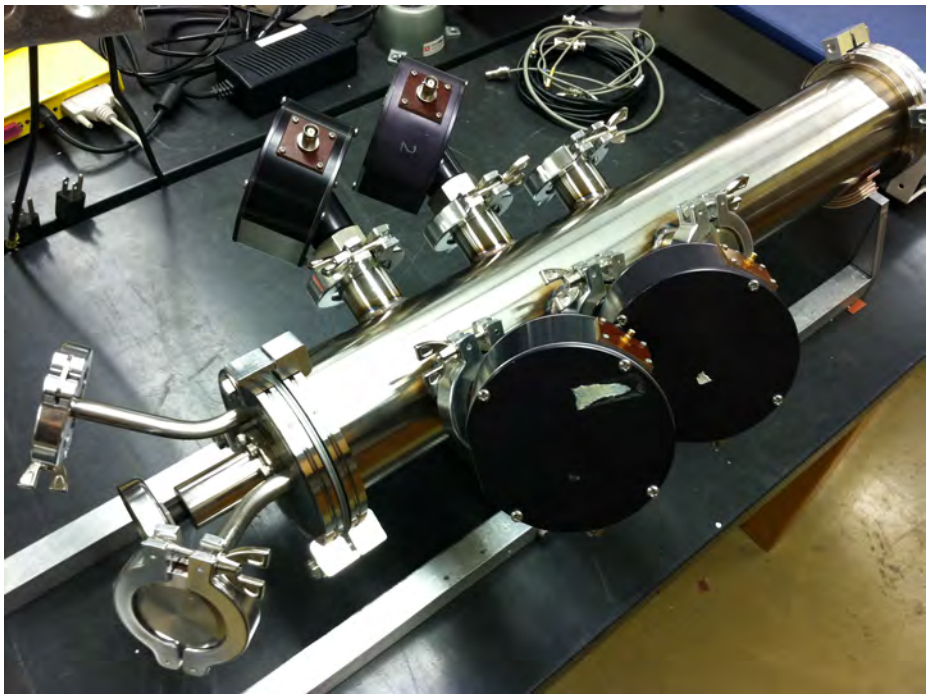

Figure 3.1: Apparatus chamber: The chamber can accommodate up to six photomultiplier tubes. Compression is applied via a knob at the left. The apparatus is supported by an aluminum frame.

Figure 3.2: Apparatus chamber while open: The inner frame of the apparatus can be moved out of the chamber for sample loading.

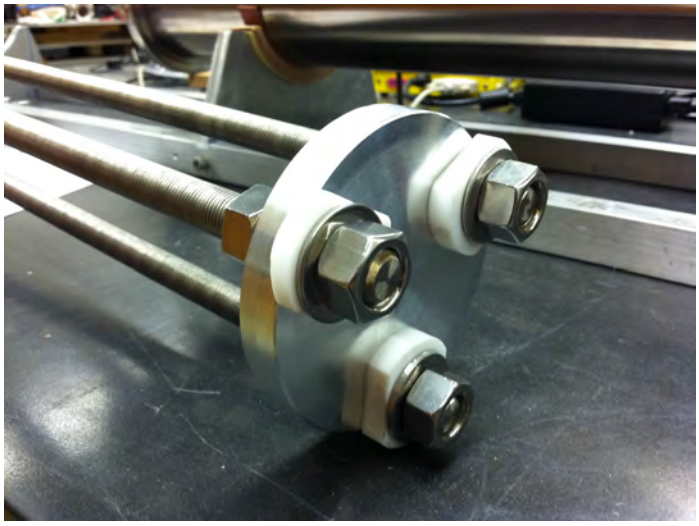

Figure 3.3: End plate to support the inner frame's weight. Three oval shaped pieces of teflon guide the frame into position in the chamber.

The machining schematic for the end flange supporting the frame is included in Appendix B (see Fig. B.1 and Fig. B.2). Two tubes were welded to the air-side of the end flange. Each tube ended in a KF40 flange which could be used for wire feedthroughs. In the center of the the end flange was a knob for applying compressional stress. The compressional knob was a modified Type L ultra high vacuum valve by Granville-Phillips. The vacuum valve had very fine threading, so small amounts of stress could be slowly applied to the sample. One platen was attached to the vacuum valve inside the chamber by a connecting rod (see Fig. B.3 in Appendix B). As the knob was turned, the platen moved and compressed the sample. A bellows maintained the vacuum seal while the platen moved. The other platen was supported by the three threaded frame rods. This platen could be adjusted to accommodate a variety of sample sizes, but it remained stationary during experimental tests. Both platens could not rotate, which was important for ensuring no shear was introduced during experimental tests.

The chamber was supported and held in place by an aluminum frame. When the chamber was open, the extended internal frame of the chamber was supported by the

aluminum support frame (see Fig. 3.2). Metal straps and clamps locked the chamber in place to facilitate sample loading and experimentation.

3.2 Acoustic Detection

Acoustic emission signals were detected by two small piezoelectric transducers placed on the platens (see Fig 3.4). When an acoustic wave reaches a transducer, the transducer is compressed and a charge difference is created across the transducer. Connecting wires to the transducer allows an acoustic wave to be detected as an electric signal. A backload was attached to the back of each transducer to ensure each transducer had enough inertia to detect the acoustic vibrations. (The transducers measure acceleration, not displacement.) The transducers and the backloads were affixed with super glue. If greater source location accuracy was required, additional transducers could be placed directly on the sample to allow for three-dimensional source location.

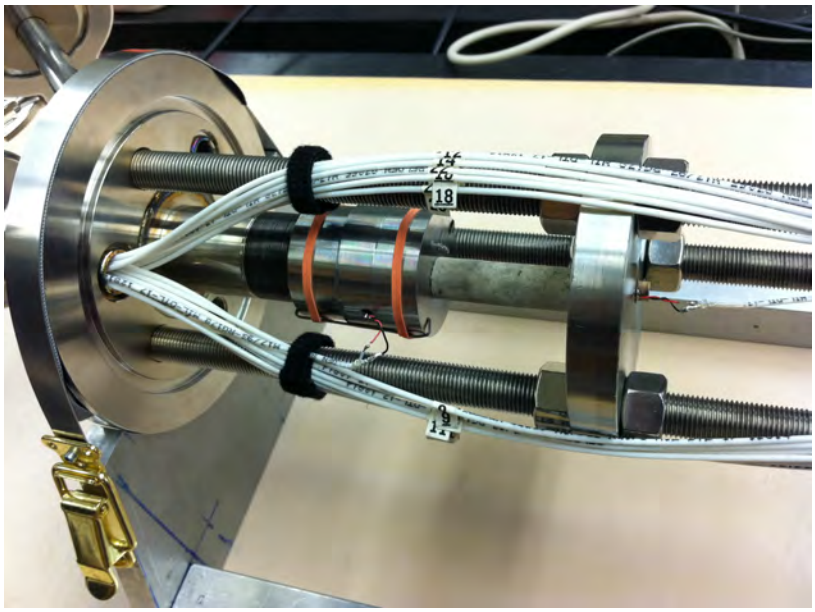

Figure 3.4: Piezoelectric transducers placed on platens: Two piezoelectric transducers detect acoustic emission. The transducer on the right is easily visible. The transducer of the left is placed inside the platen.

3.3 Light Detection

Photomultiplier tubes (PMTs) allow low levels of light to be detected with a high temporal accuracy. Six 7767 type PMTs are positioned along the chamber and oriented to directly face the rock sample. The PMTs have a spectral response of roughly 300-600nm and an electron-transit time of 20 ns. The PMTs are removable, and a spectrometer could be positioned in their place to measure the spectral output of the ML. Only two PMTs are necessary when measuring samples shorter than 3 in. Four PMTs are recommended for samples measuring between 3 in. and 4 in., and all six PMTs should be used for samples longer than 7 in. in length.

A SRS high voltage power supply was used to power the PMTs. A series of resistors distributes the voltage among the cathode and the 10 dynodes of the PMT (see Fig. A.1 in Appendix A). The PMT circuit board requires negative polarity from the high voltage power supply, and great care was taken to ensure the negative polarity was used to avoid damaging the PMTs. The PMTs were only powered in dark environments, as over saturation can also cause damage.

Care was taken to ensure the chamber was light-tight after a sample was loaded. The chamber could be conveniently tested for a light-tight seal by turning the room lights on and off and by shining a flashlight at possible light leak locations on the chamber. If a light leak was present, the voltage output of the PMTs would respond readily to a change in lighting conditions.

Before any experiment was performed, the PMTs were tested to ensure they were functioning properly. A fiber optic cable fed light from a flashlight into the chamber through an unused PMT port (see Fig. 3.5). The flashlight could be rapidly turned on and off to provide a small, consistent source of light.

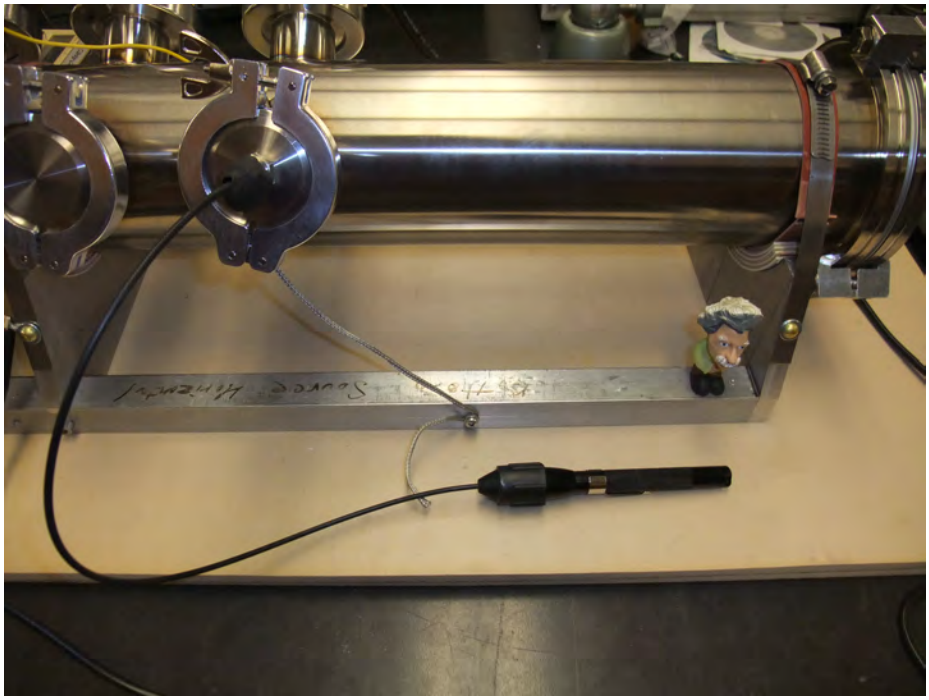

Figure 3.5: PMT light test system: A flashlight connected to a fiberoptic cable allowed for convenient PMT functionality tests.

3.4 Stress and Strain Measurements

The amount of fracturing and deformation of the sample can not be directly observed during an experiment. Therefore, strain measurements provided useful information about the extent of sample deformation. Strain is a measure of the change in length of a sample when stress is applied. Strain is defined as

$$e = \frac{L_f - L_0}{L_0}, \tag{3.1}$$

where L_0 is the initial length of the sample and L_f is the length of the sample after deformation. The initial sample length L_0 was measured before loading the sample. The change in sample length, L_f, was determined during the course of the experiment by measuring the amount the anvil knob was turned. A protractor and an arrow affixed to the end of the apparatus allowed rotation of the knob to be

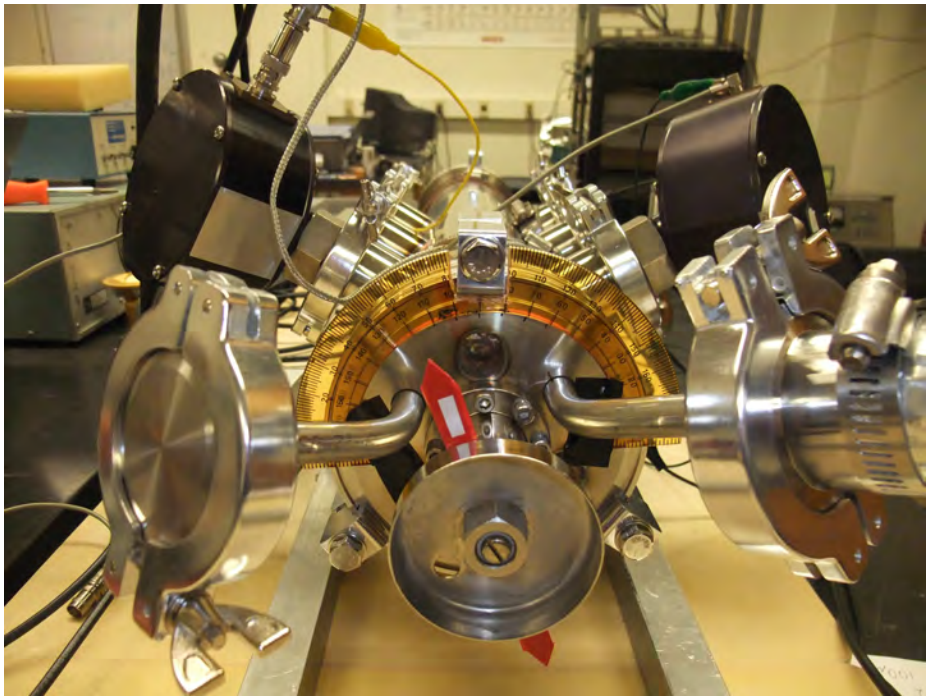

Figure 3.6: Strain measurement system: A protractor and red arrows were used to quantify the amount the anvil knob was rotated during an experiment.

measured accurately to 5°. The pitch of the thread of the anvil was measured to be 0.625mm/turn. Therefore, for every 5° of rotation, the sample was compressed approximately 8.7μm. For a sample measuring 50 mm in length, a 5° turn of the knob strained the sample 0.2 milli-strains.

3.5 Data Acquisition

Signals were sent from the photomultiplier tubes and the piezoelectric transducers with coaxial cables to avoid cross-talk. Each signal was first amplified with a Cremat CR-112 charge amplifier. The circuit design is shown in Fig. A.2 in Appendix A. A small stainless steel box with BNC connectors for input, output, and voltage supply was designed and built to house four CR-112 charge amplifiers (see Fig. 3.7).

After amplification, signals were recorded with oscilloscopes. A Tektronix TLS

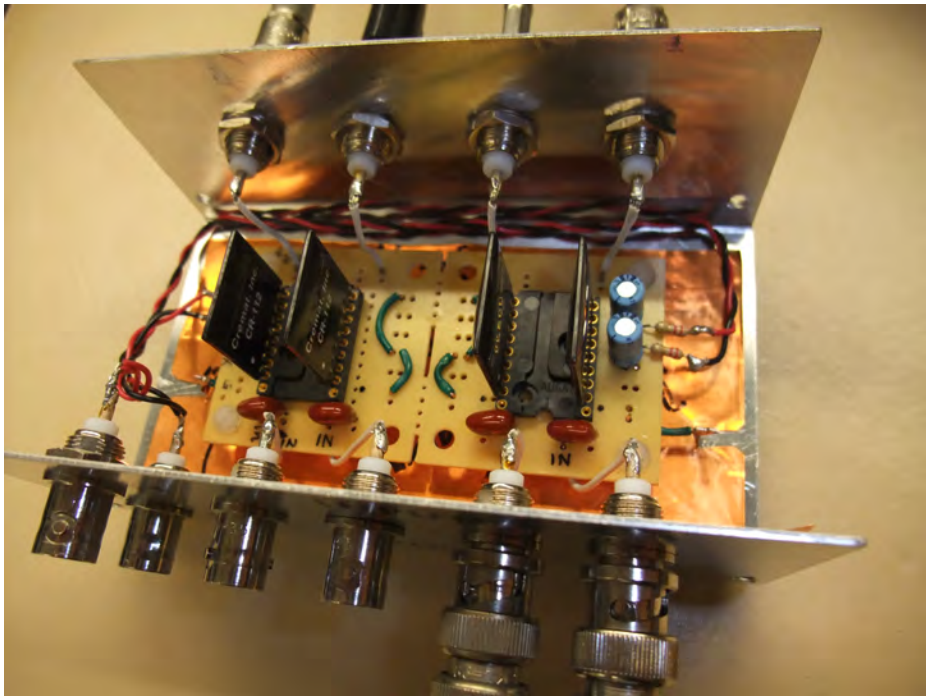

Figure 3.7: Charge amplifier box: The interior of the box contains four Cremat charge amplifiers.

216 oscilloscope and a Tektronix TDS 1002 oscilloscope were used. Because the aim of this project was to study correlation in time, it was important that both oscilloscopes collected data at the same time. It was quickly realized that the oscilloscopes and the computer did not have enough memory to continuously collect data at high temporal resolution over the length of time required to perform an experiment. The best option was to record discrete events at a high temporal resolution.

The TLS 216 can output its trigger signal but cannot trigger off an external source, and the TDS 1002 can trigger off an external source but cannot output its trigger source. Therefore, the TLS 216 oscilloscope was chosen to trigger off an event while the TDS 1002 oscilloscope was triggered by the TLS 216.

Two different setups were used. In the first setup, sound was measured with the TLS 216, and light was measured with the TDS 1002. Whenever a burst of *sound* was detected, both oscilloscopes would trigger and record data for a short amount of time.

In the second setup, light was measured with the TLS 216, and sound was measured with the TDS 1002. Whenever a large burst of *light* was detected, both oscilloscopes would trigger and record data for a small duration of time. Tests on sugar cubes (see Section 5.2) were most successful when triggering off ML, while tests on rock tended to be most successful when triggering off AE events. The reason for this observation is that sugar emits a large amount of ML but has a very high attenuation, while AE was detected much more frequently than ML in rock. Each measurement was then sent to a computer with GPIB and saved with LabVIEW.

Chapter 4

Experimentation

4.1 Procedures

The dimensions of each sample were measured before the experiment began. The sample was then centered between the two compressional platens. After closing and tightening the chamber, a voltage of 1200 V was supplied to the PMTs. The chamber was tested for light leaks, and the PMTs and piezoelectric transducers were tested for proper functionality. The initial position of the knob was recorded.

The compressional knob was slowly rotated with a wrench for greater precision. When the wrench tapped the chamber, a large acoustic wave was detected by the transducers. To avoid acoustic interference during the experiment, the wrench was wrapped in electrical tape to eliminate this effect. Whenever an event was detected, the transducer and PMT data were saved and the strain was recorded. The sample was commonly fractured during the experiment.

4.2 Mechanoluminescence Preliminary Tests

The rock core samples available for this study were limited, so it was important to ensure the instrument was operating properly before testing the rock samples. When crushed, sugar produces a brilliant mechanoluminescence that can been seen by the

unaided eye in a dark room. Francis Bacon wrote in 1620 in *Novum Organum*,[1] "It is also most certain that all sugar, whether refined or raw, provided only it be somewhat hard, sparkles when broken or scraped with a knife in the dark" [2, p. 312]. Robert Boyle also noted in 1660 "that hard sugar, being briskly scraped with a knife, affords a sparkling light" [13, p. 510]. Sugar cubes are inexpensive, and they are quite similar to sandstone in that they are an aggregate of smaller grains. A study by Dickinson et al. [5] looked at fracto-emission (particle and light emission from fractured surfaces) of various materials. They found both quartz and crystalline sugar emitted 10^6 electrons per cm^2 of fractured surface and had a comparable fracto-emission decay rate. Sugar cubes, therefore, were particularly useful for simulating sandstone during preliminary testing of the photomultiplier tubes.

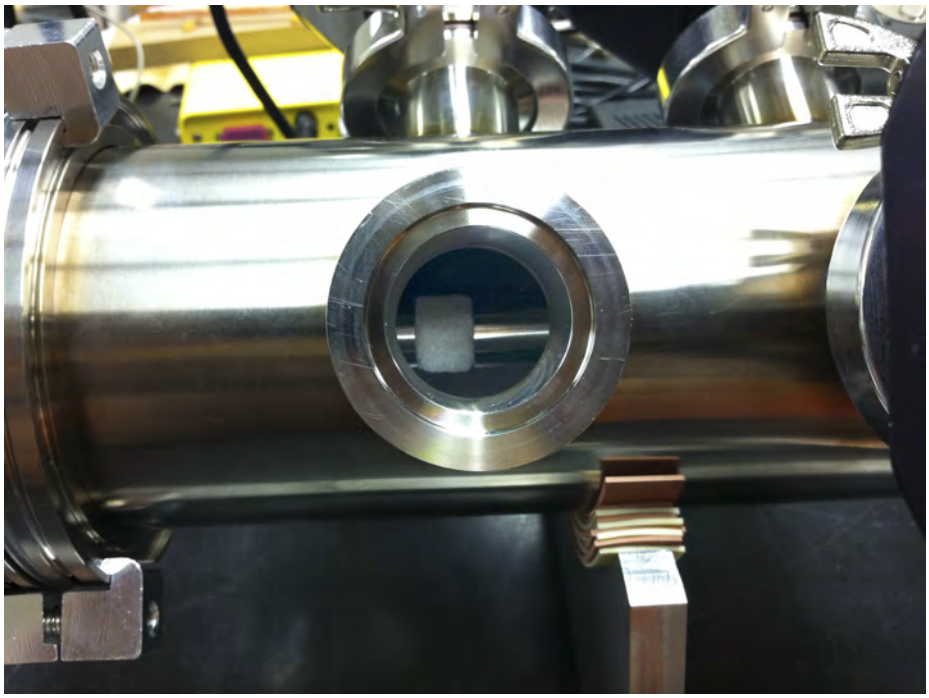

Figure 4.1: A sugar cube used for ML detection testing purposes can be seen viewed through a PMT port.

[1]Several sources, including B. P. Chandra's chapter in *Luminescence of Solids* [16], attribute Francis Bacon's reference about the emission of light from sugar to *Of the Advancement of Learning*. However, Bacon's reference actually appeared in *Novum Organum*. Chandra also accidentally attributes Robert Boyle's quote about sugar to Francis Bacon.

Fig 4.1 shows a sugar cube in the chamber as seen from a PMT port. Sugar cubes have a remarkably high attenuation and, unlike sandstone, are very soft. Therefore, they were not adequate for testing the functionality of the piezoelectric transducers. A measurement of ML and AE from a sugar cube is shown in Fig. 4.2. Note the sharp ML peaks in the top two plots and the attenuated AE signal in the bottom two plots.

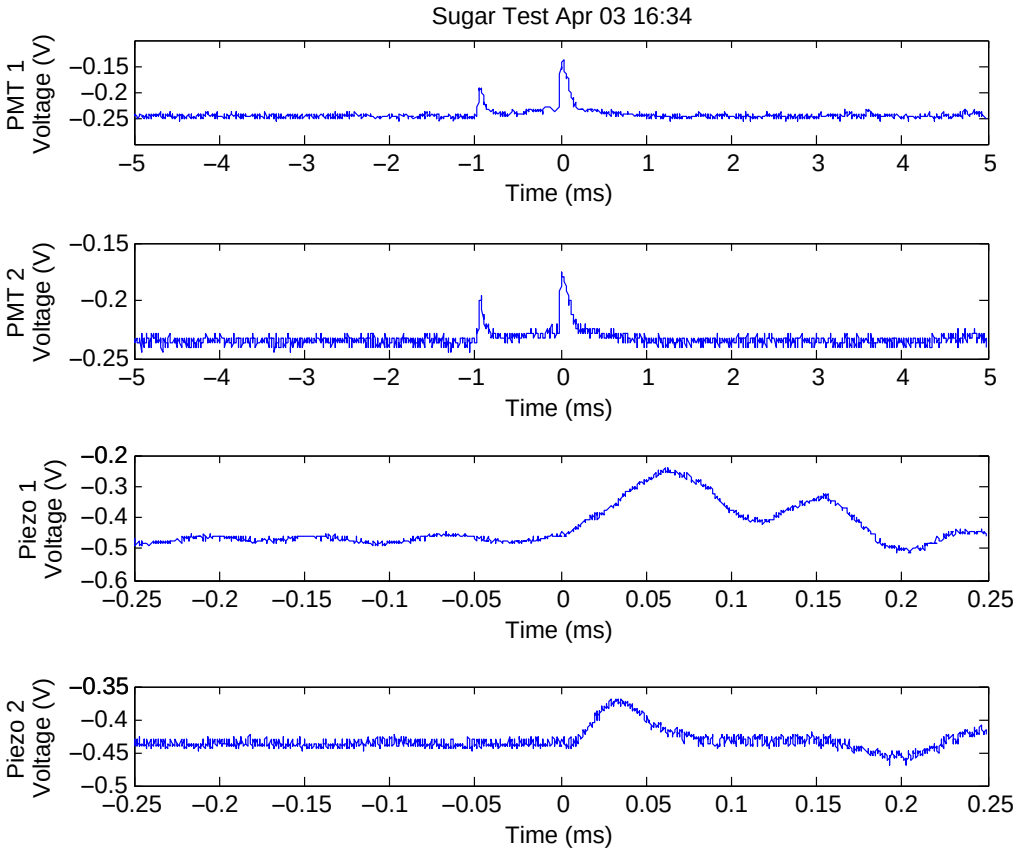

Figure 4.2: ML and AE plots from a sugar cube: The top two plots show ML peaks measured by two PMTs. The bottom two plots show the corresponding AE emission measured by two piezoelectric transducers. Piezo 1 was attached to the stationary platen, and piezo 2 was attached to the compressing platen (see Fig. 5.1). All four measurements were triggered by PMT 1 (the top plot), and all measurements were triggered at 0 ms (in the center of the plots). The top two plots span a larger segment of time than the bottom two plots, so the ML peaks detected at -1 ms are outside the field of view of the bottom two plots.

4.3 Acoustic Emission Preliminary Tests

Acoustic emission can be simulated by breaking a piece of pencil lead directly on the rock core. This technique, known as the pencil lead break (PLB) technique, involves using a mechanical pencil with a few millimeters of pencil lead protruding out [7]. The pencil lead is forced against the sample until the pencil lead breaks and an acoustic wave is sent through the sample. The acoustic wave created by the PLB technique closely approximates an acoustic emission signal created during sample deformation. Therefore, the PLB technique is useful for testing the functionality of the piezoelectric transducers.

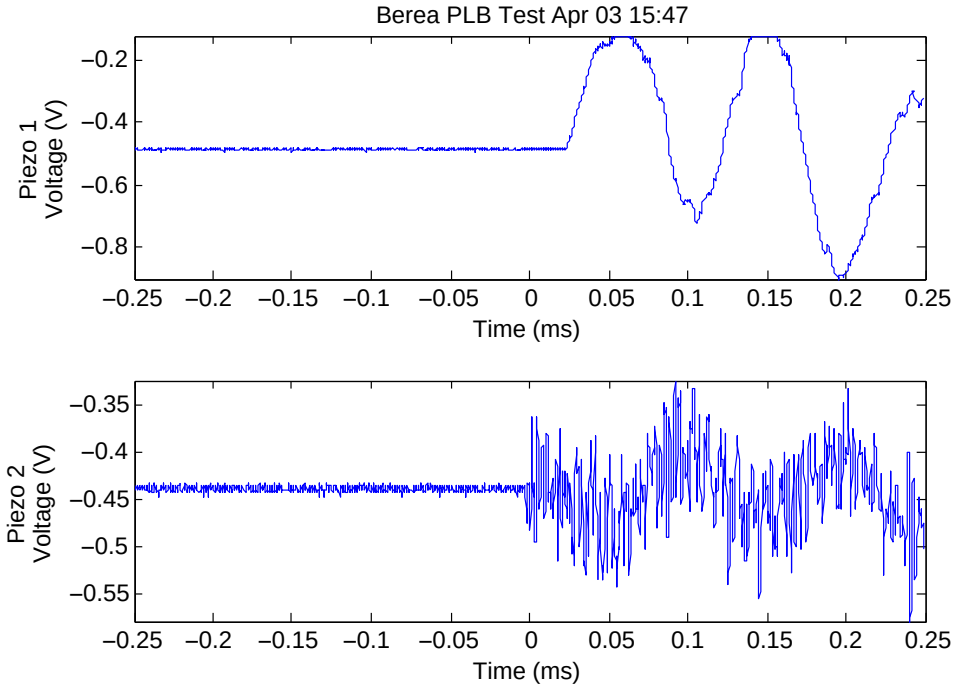

Figure 4.3: Acoustic wave plots for determining the sound velocity of Berea: The plots show acoustic waves measured by two piezoelectric transducers. The acoustic waves were caused by a piece of pencil lead breaking on a Berea sandstone sample close to piezo 2 (bottom plot). Because the source location was known, the difference in arrival time was used to determine the sound velocity of the Berea sample. The difference in peak shape between the top and bottom graph is a result of attenuation in the sample and in the platens. Piezo 1 was attached to the stationary platen, and piezo 2 was attached to the compressing platen (see Fig. 5.1).

Because the source position of the PLB technique is known, this technique is also particularly convenient for measuring the sound velocity of a given sample. To measure the sound velocity of a sample, the pencil lead was broken at the very end of a sample to yield the maximum difference between acoustic wave arrival times. The greater the difference was between arrival times, the more accurate the sound velocity calculation would be. Pencil lead sizes of 0.7 mm, 0.5 mm, and 0.3 mm were used for functionality tests and sample sound velocity measurements. Thicker pencil lead produces larger amplitude acoustic waves, so a variety of pencil lead sizes were used to simulate a variety of AE amplitudes. An acoustic wave from a sound velocity measurement is plotted in Fig. 4.3.

4.4 Berea Sandstone Test

A Berea sandstone core measuring 45 mm in length was compressed, and acoustic emission and mechanoluminecence events were measured. The measurements were triggered by the AE events. A total of 32 AE events were recorded, and 19 of those AE events were accompanied by ML. An example of the AE and ML plots is shown in Fig. 4.4. Because many peak picking programs can incorrectly determine the arrival time of acoustic signals, the arrival times of each AE and ML peak were found by hand. The AE sources were located spatially and temporally by the method outline in Section 1.2. Because the rock was slowly compressed, the length of the core changed over time. Sample length change was accounted for in the source position and time calculations.

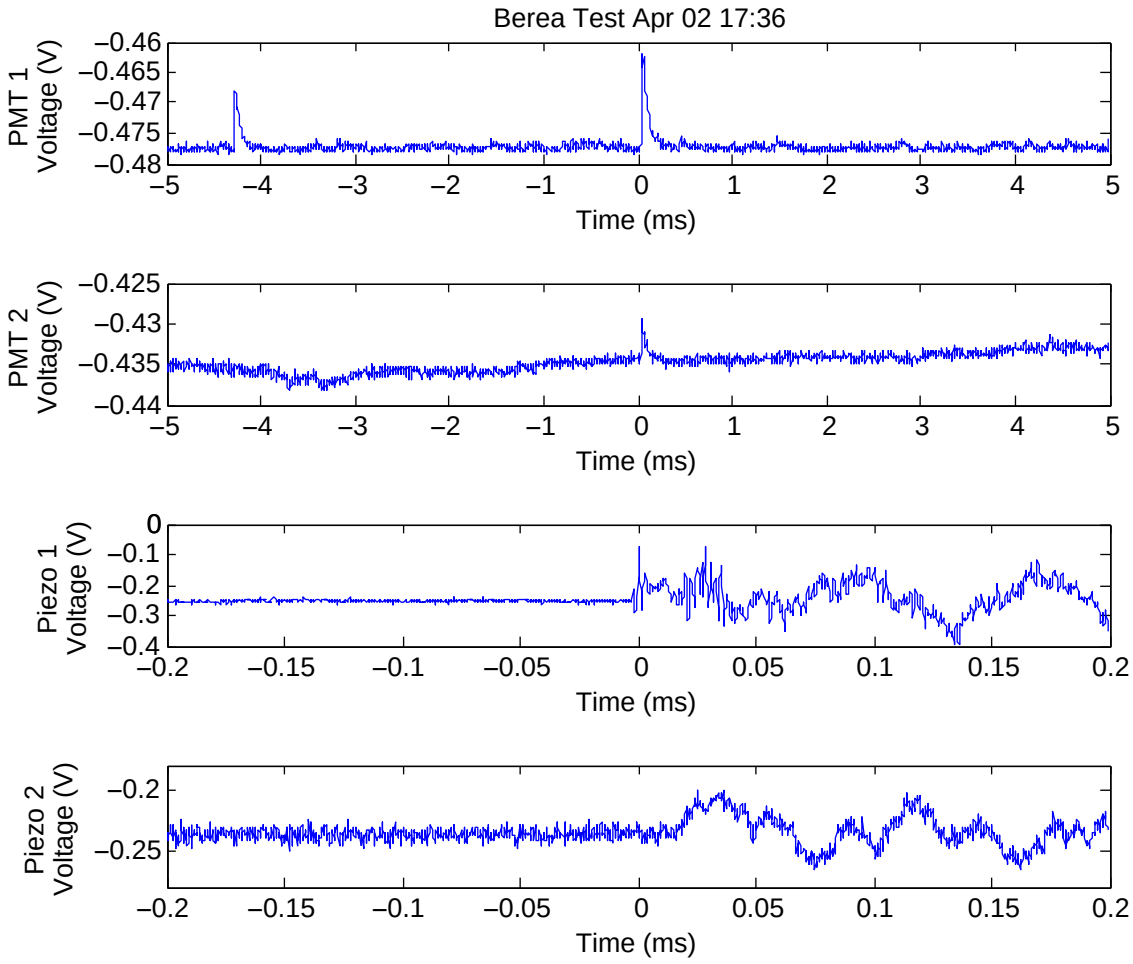

Figure 4.4: ML and AE plots from a Berea sandstone core: The top two plots show ML peaks measured by two PMTs. The bottom two plots show the corresponding AE emission measured by two piezoelectric transducers. Piezo 1 was attached to the stationary platen, and piezo 2 was attached to the compressing platen (see Fig. 5.1). All four measurements were triggered by piezo 1 (the third plot from the top), and all measurements were triggered at 0 ms (in the center of the plots). The top two plots span a larger segment of time than the bottom two plots, so the ML peak detected near -4 ms is outside the field of view of the bottom two plots.

Chapter 5

Results and Conclusion

5.1 Sound Velocity Determination

Several pencil lead break (PLB) tests were performed on a Berea sandstone core to determine the sound velocity of the core. The core measured 50.0 mm in length. Pencil lead was broken at the core/platen interfaces near piezo 1 and at the core/platen interface near piezo 2. The PLB tests near piezo 1 yielded an average sound velocity of 1533 m/s, and the PLB tests near piezo 2 yielded an average sound velocity of 1995 m/s (see Table 5.1). The large difference in measured sound velocity could be due to the response of the piezoelectric transducers or due to attenuation within the Berea sample. Because the tests conducted near piezo 10 had a smaller standard deviation (46.8 m/s) and shorter dt values, the PLB test near piezo 10 is believed to be more accurate. Therefore, 1995 m/s was used for the sound velocity of Berea sandstone in later calculations.

Table 5.1: Arrival times, difference in arrival times, and calculated sound velocity for four tests on a Berea sandstone core measuring 50.0 mm in length. Sound velocity was calculated with Eq. 1.8.

Pencil lead broken near piezo 1

Test	Pencil Lead	Piezo 1 Arrival Time	Piezo 2 Arrival Time	dt	Sound Velocity
1	0.7 mm	237.2 μs	268.2 μs	31.0 μs	1598.6 m/s
2	0.7 mm	246.4 μs	281.0 μs	34.6 μs	1433.6 m/s
3	0.5 mm	248.2 μs	277.0 μs	28.8 μs	1719.5 m/s
4	0.3 mm	248.4 μs	284.4 μs	36.0 μs	1378.3 m/s
Avg				32.6 μs	1532.5 m/s
Std Dev				3.3 μs	155.9m/s

Pencil lead broken near piezo 2

Test	Pencil Lead	Piezo 1 Arrival Time	Piezo 2 Arrival Time	dt	Sound Velocity
1	0.7 mm	273.8 μs	247.6 μs	26.2 μs	1928.8 m/s
2	0.7 mm	272.8 μs	248.0 μs	24.8 μs	2039.0 m/s
3	0.5 mm	244.6 μs	219.4 μs	25.2 μs	2006.2 m/s
4	0.3 mm	214.0 μs	188.8 μs	25.2 μs	2006.2 m/s
Avg				25.4 μs	1995.1 m/s
Std Dev				0.6 μs	46.8 m/s

5.2 AE Source Location

The AE source positions from the Berea sandstone core are plotted in Fig. 5.1. The AE events are clustered closely at one end of the core. Later examination of the core revealed these AE source locations closely match the actual location where the sample fractured. Several AE events positions were calculated to be inside the platen. These AE events likely occurred at the core/platen boundary. Source location error is a result of error in the sample sound velocity determination and error in picking AE arrival times.

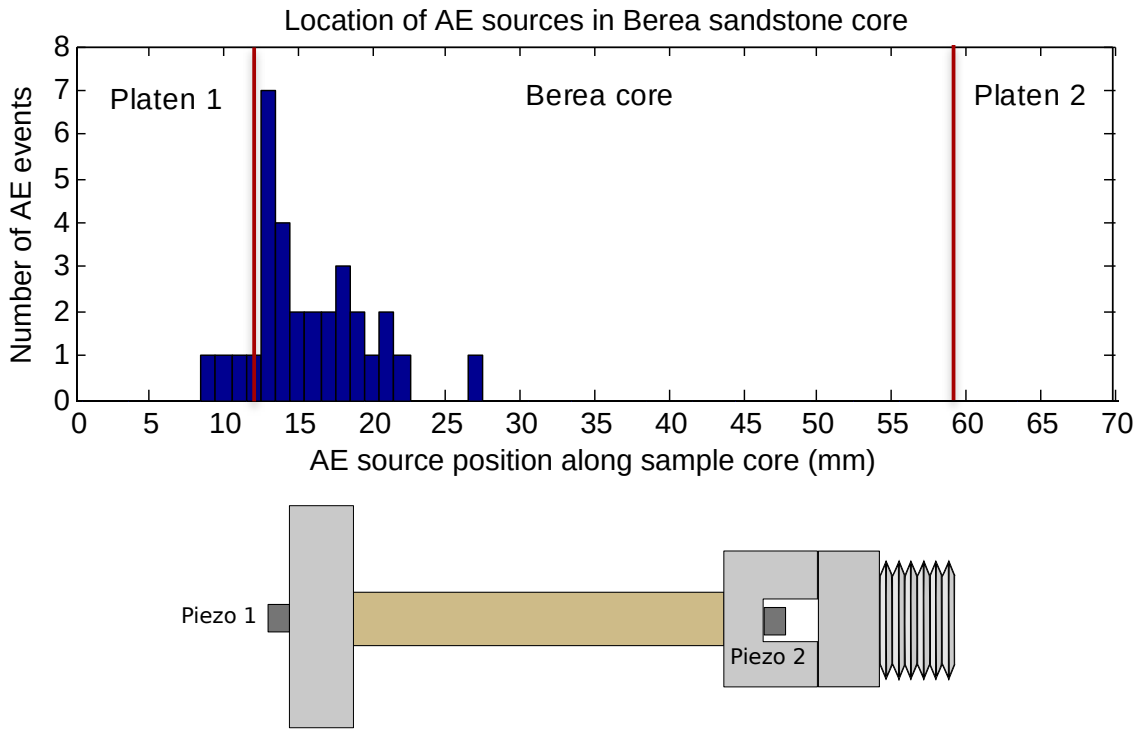

Figure 5.1: AE source locations in a Berea sandstone core. Platen/core interfaces are marked in red.

5.3 AE and ML Correlation

AE source locations, AE source times, and ML source times are plotted in Table 5.2. Most notably, the ML events occur approximately 40 μs after the AE events. ML events were only observed after the Berea sandstone core began to fracture. Berea sandstone has a large clay content and absorbs visible light remarkably well. It is likely that light emission on the surface was necessary for ML detection. Fractures would create more surface area and likely expose event locations. The sandstone core did not fall from the platens after fracturing due to a small amount of backlash in one platen. While the platen backlash introduced some inaccuracy in the strain calculation, the backlash allowed continued compression of the Berea core after fracturing had already occurred and allowed extensive observation of ML.

The repeated ∼40 μs delay between AE and ML is quite unexpected. Perhaps ML is emitted after stress has been released and the sample relaxes. Frictional rubbing between grains and fractured surfaces may occur as stress is released. Fractures in piezoelectric material may also be responsible for this effect. Perhaps fractures open over several microseconds rather than instantaneously. These AE and ML results are preliminary, and further tests are necessary to narrow possible ML source mechanisms. Further tests are also necessary to eliminate the possibility that this ∼40 μs delay is caused by backlash of the compressing platen.

Table 5.2: AE source locations, AE source times, ML source times, and strain are tabulated for a Berea sandstone core measuring 50.0 mm in length. Each ML event appears to have occurred approximately 40 μs before the corresponding AE event occurred.

Time	AE Source Location	AE Source Time	ML Time	ML Time - AE Time	Milli-Strain
17:08	8.8 mm	-26.7 μs	12 μs	39 μs	-8.5
17:10	10.9 mm	-30.7 μs	8 μs	39 μs	-10.8
17:12	12.9 mm	-4.1 μs	36 μs	40 μs	-13.1
17:14	14.2 mm	-3.1 μs	36 μs	39 μs	-17.7
17:17	13.2 mm	-14.2 μs	24 μs	38 μs	-18.5
17:27	12.5 mm	-2.3 μs	36 μs	38 μs	-32.2
17:30	14.6 mm	-5.8 μs	36 μs	42 μs	-32.4
17:33	12.7 mm	-4.0 μs	36 μs	40 μs	-37.6
17:34	12.5 mm	-32.1 μs	36 μs	68 μs	-38.0
17:35	14.3 mm	-28.4 μs	8 μs	36 μs	-38.4
17:36	13.3 mm	-4.7 μs	12 μs	17 μs	-39.2
17:41	12.9 mm	-31.3 μs	8 μs	39 μs	-49.4
17:43	14.6 mm	-33.3 μs	12 μs	45 μs	-53.6
17:45	17.7 mm	-6.9 μs	32 μs	41 μs	-54.2
17:49	17.8 mm	-6.8 μs	36 μs	45 μs	-68.3
17:51	15.9 mm	-5.4 μs	32 μs	37 μs	-74.1
17:52	17.1 mm	-6.2 μs	36 μs	42 μs	-74.5
17:54	16.8 mm	-4.5 μs	4 μs	8 μs	-76.8
17:55	17.6 mm	-7.0 μs	36 μs	43 μs	-80.2

5.4 Suggestions for Future Work

Additional work is necessary to narrow possible ML source mechanisms. A comparison of AE and ML from various rocks would provide valuable information about ML mechanisms. Additionally, ML may be more easily measured from samples with less light absorption such as a quartz arenite or a clean marble. The spectra of ML emission could be studied by connecting a spectrometer to one of the PMT ports and integrating over time. Repetition of similar experiments under vacuum and in various gases would provide additional information about the mechanism behind ML. The correlation of AE and ML could be improved by measuring AE and ML on the same time scale. To increase the accuracy of AE source location, additional piezoelectric transducers could be attached to the sample.

A more accurate strain measurement could be obtained through the use of strain gauges. Measuring the stress of the sample would provide useful stress-strain curves. Stress could be detected by measuring the application of torque to the compression knob. Another method of measuring stress involves placing a material with a known stress-strain curve in-line with the sample. As the system is compressed, this material and the sample would experience the same stress. The strain of the material with a known stress-strain curve could be measured with a strain gauge, and the stress of the system could then be calculated. A more accurate method of evenly and slowly applying stress to the sample would also improve measurements.

5.5 Conclusions

An apparatus has been successfully designed and constructed to measure mechanoluminescence and acoustic emission from rock cores under quasistatic compression. AE measurement has been tested with the PLB method, and ML measurement has been

tested with sugar cubes. Most significantly, a correlation between ML and AE from a Berea sandstone core has been observed. Many AE events were detected without ML. This indicates either that AE events can occur without ML or that the ML events were too small to be detected. Because the oscilloscopes were triggered by AE data, it is not yet known whether ML events can occur independently of AE.

Preliminary results suggest that when AE and ML events occur together in Berea sandstone, the ML events occur approximately 40 μs after the AE events. This is a remarkably long delay time for the system. For a sample of Berea sandstone measuring 50 mm in length, a compressional acoustic wave only takes about 25 μs to travel from one end of the sample to the other end. It is still too early to provide a reasonable mechanism for the $\sim$40 μs delay between AE and ML. These are interesting results, but they require confirmation with other data. Luckily, the recently constructed apparatus can be used to gain extensive additional information about ML and AE in Berea sandstone and other geologic materials.

References

[1] N. W. Ashcroft and N. D. Mermin. *Solid State Physics*. Brooks/Cole, Belmont, CA, 1976.

[2] F. Bacon. *The Philosophical Works of Francis Bacon*. Books for Libraries Press, Freeport, New York, 1970.

[3] B. P. Chandra. Acoustic and photon emissions during mechanical deformation of coloured alkali halide crystals. *Journal of Physics D: Applied Physics*, 17:117–123, 1984.

[4] G. N. Chapman and A. J. Walton. Triboluminescence of glasses and quartz. *Journal of Applied Physics*, 54(10):5961–5965, 1983.

[5] J. T. Dickinson, E. E. Donaldson, and M. K. Park. The emission of electrons and positive ions from fracture of materials. *Journal of Materials Science*, 16:2897–2908, 1981.

[6] N. C. Eddingsaas and K. S. Suslick. Mechanoluminescence: Light from sonication of crystal slurries. *Nature*, 444:163, Nov. 2006.

[7] R. H. Hardy. *Acoustic Emission/Microseismic Activity*. Swets & Zeitlinger B.V., Lisse, The Netherlands, 2003.

[8] C. Kittel. *Introduction to Solid State Physics*. John Wiley and Sons, Inc., Hoboken, NJ, 8 edition, 2005.

[9] C. Klein and B. Dutrow. *Mineral Science*. John Wiley and Sons, Inc., Hoboken, NJ, 2007.

[10] R. G. Liptai, editor. *Acoustic Emission*. American Society for Testing and Materials, 1972.

[11] F. R. Redfern and R. D. Munson. *Acoustic emission source location: A mathematical analysis*. University of Michigan Library, 1982.

[12] G. T. Reynolds. Piezoluminescence from a ferroelectric polymer and quartz. *Journal of Luminescence*, 75:295–299, 1997.

[13] P. Shaw. *The Philosophical Works of the Honorable Robert Boyle, Volume 2.* London, 1725.

[14] L. M. Sweeting and J. L. Guido. An improved method for determining triboluminescence spectra. *Journal of Luminescence*, 33:167–173, 1985.

[15] P. A. Tipler and G. Mosca. *Physics for Scientists and Engineers.* W. H. Freeman and Company, New York, 5 edition, 2004.

[16] D. R. Vij, editor. *Luminescence of Solids.* Plenum Press, 1998.

[17] T. Wedgwood and J. Banks. Experiments and observations on the production of light from different bodies, by heat and by attrition. *Philosophical Transactions of the Royal Society of London*, 82:28–47, Jan. 1792.

Appendix A

Circuit Schematics

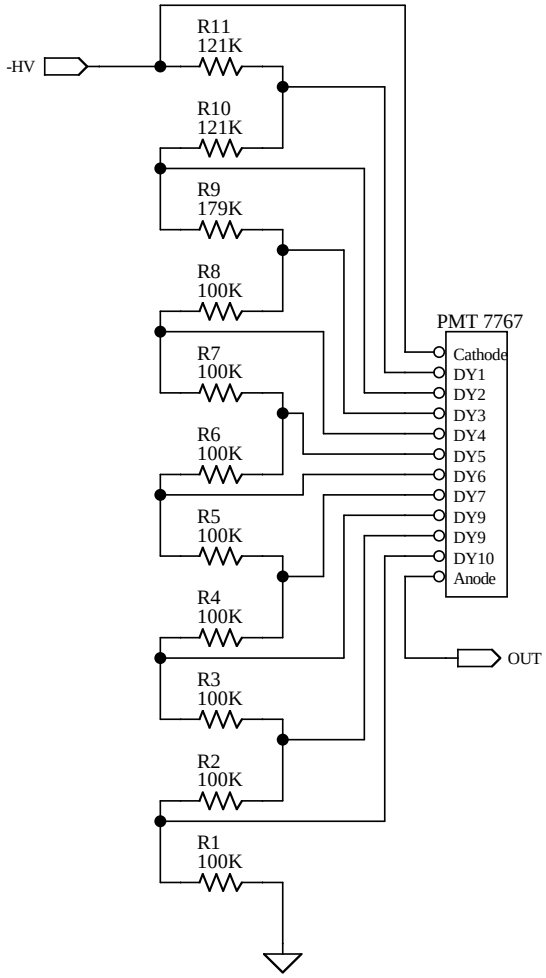

Figure A.1: A series of resistors distributes high voltage across a photomultiplier tube's cathode and dynodes

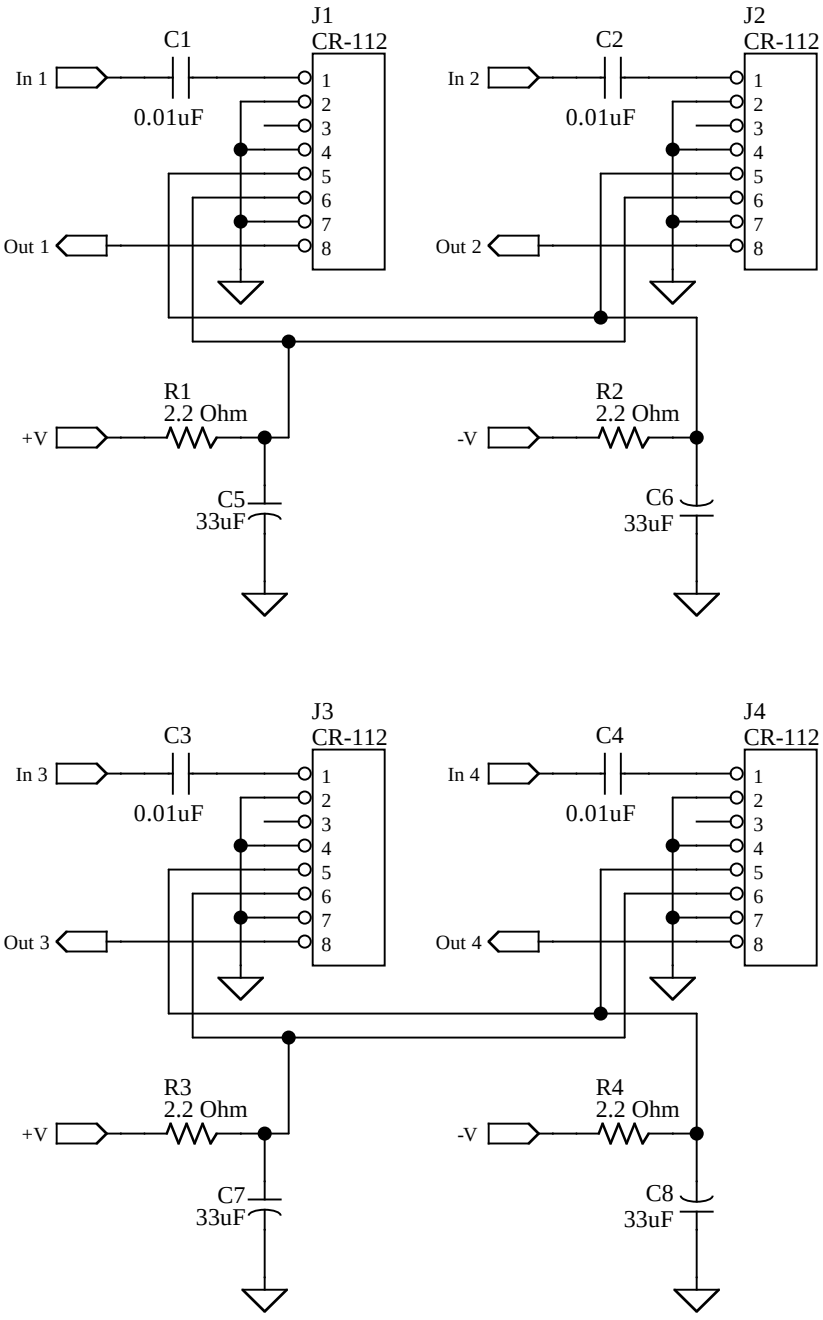

Figure A.2: Circuit layout for four charge amplifiers. Signals from the photomultiplier tubes and the piezoelectric transducers are amplified before they are measured by the oscilloscopes.

Appendix B

Instrument Design Schematics

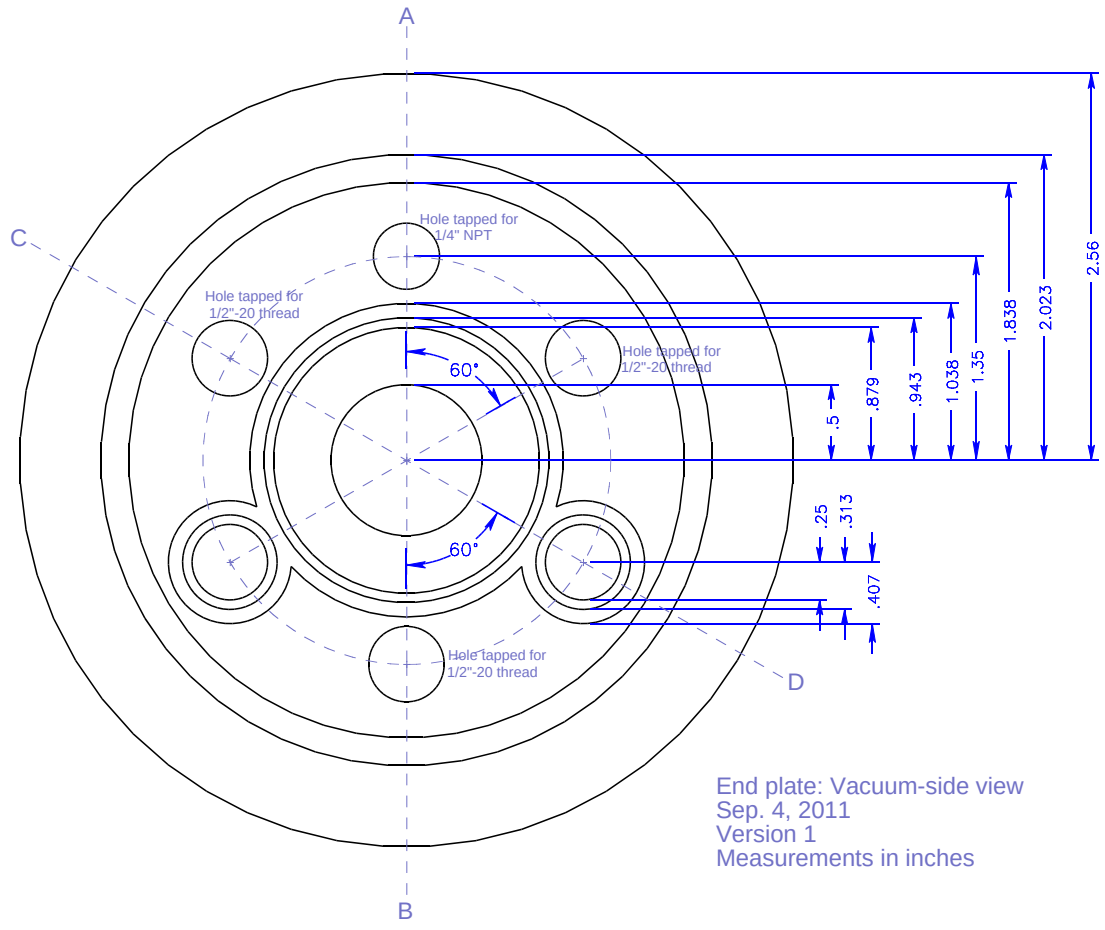

Figure B.1: The end vacuum flange viewed from the vacuum side

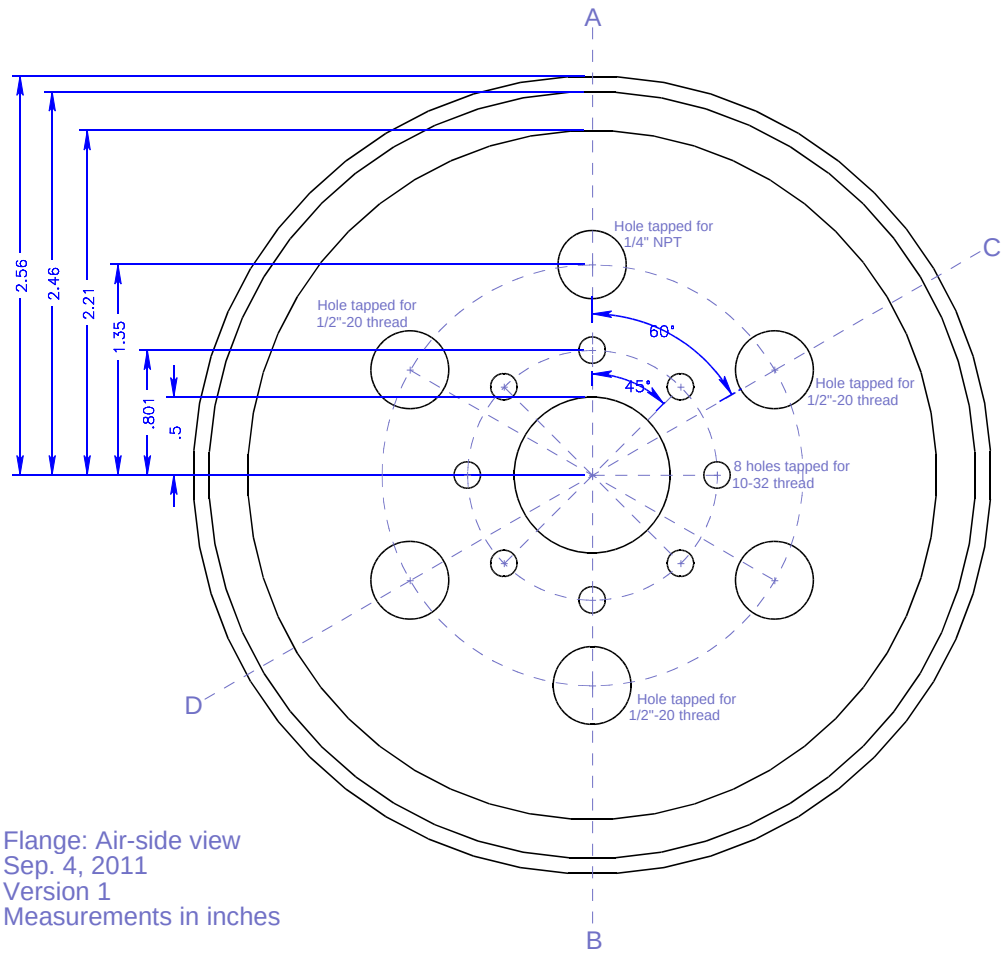

Figure B.2: The end vacuum flange viewed from the air side

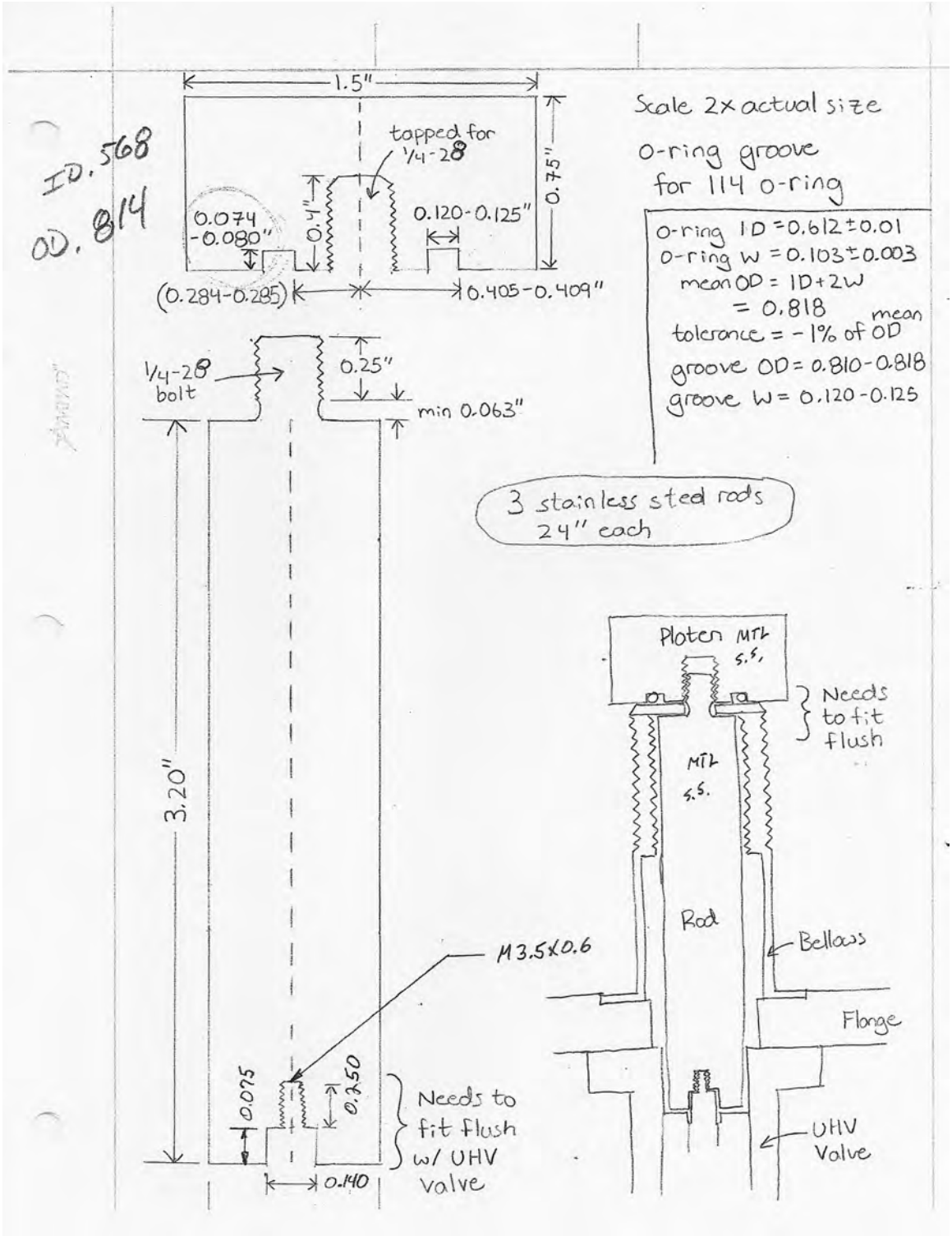

Figure B.3: The platen and rod which connect to the UHV valve and apply stress to the sample

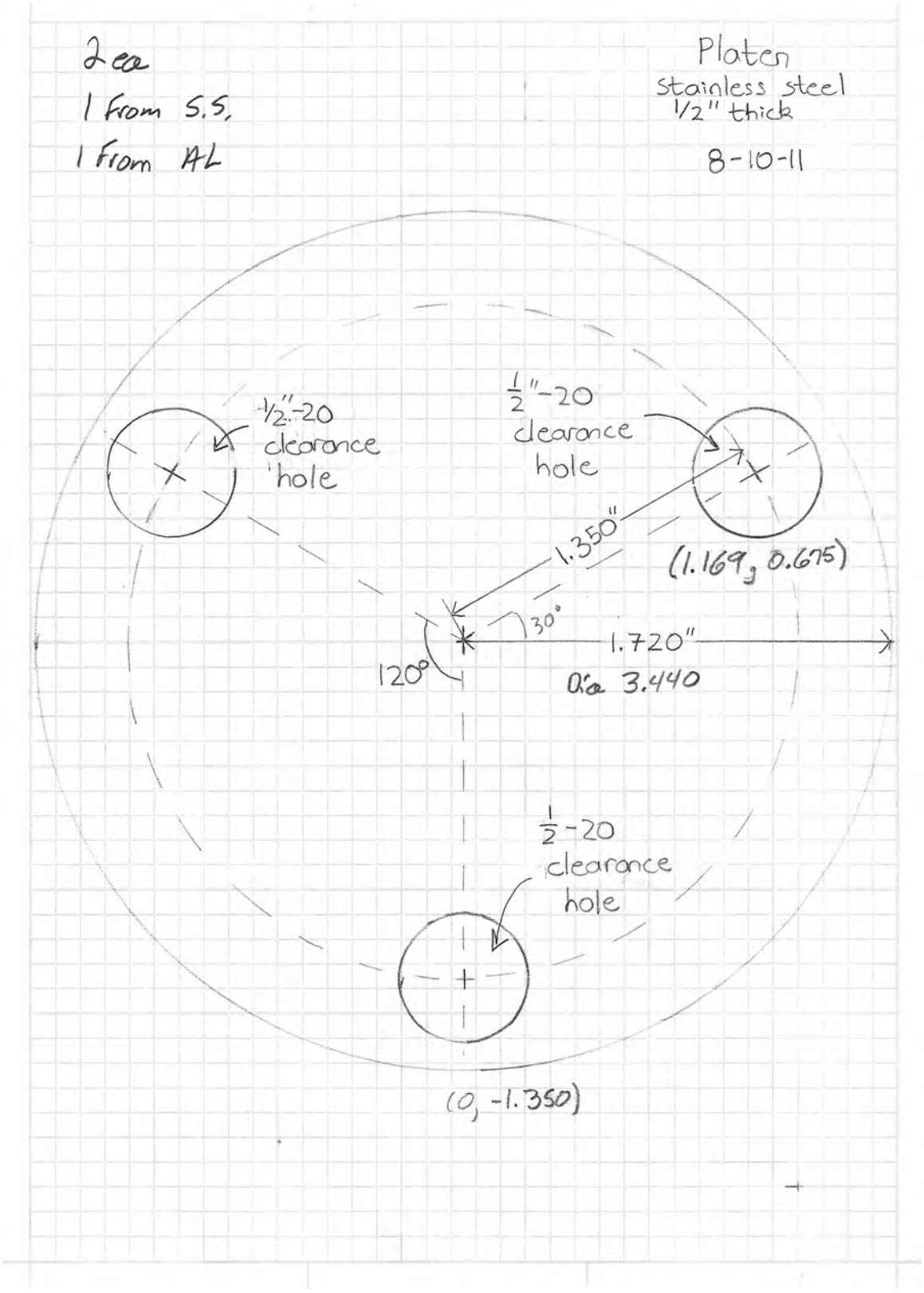

Figure B.4: The platen connected to the inner frame of the chamber

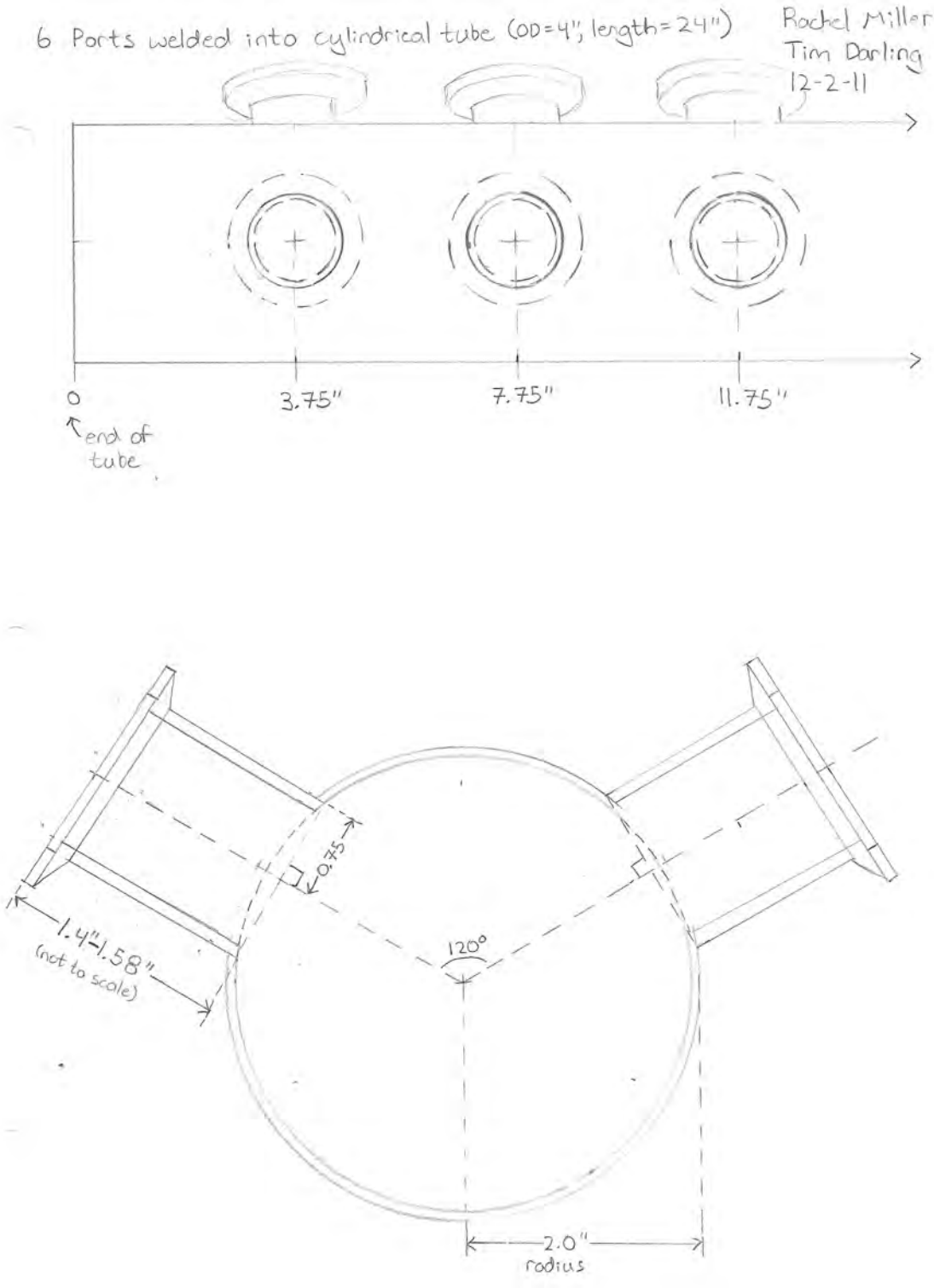

Figure B.5: PMT port location on the chamber